Korean J. Chem. Eng., 37(7), 1195-1198 (2020)
DOI: 10.1007/s11814-020-0513-6

pISSN: 0256-1115
eISSN: 1975-7220

Utilization of cross-linked polybutadiene nanoparticles for asymmetric membrane synthesis

Mehrdad Manteghian† and Farzaneh Sayyahpour

Faculty of Chemical Engineering, Tarbiat Modares University, Tehran, Iran
(*Received 16 September 2019 • Revised 9 February 2020 • Accepted 11 February 2020*)

Abstract−This research synthesized polybutadiene nanoparticles and investigated the induction time for their nucleation under different supersaturations and their cross-linking to be utilized in an asymmetric membrane synthesis. Purchased (bulk) polybutadiene was dissolved in toluene and then ethanol was added dropwise to the solution as an anti-solvent. The induction time, i.e., the time interval between adding the last drop of ethanol till appearance of a turbidity due to polybutadiene nucleation, was determined. The nucleation mechanism was investigated. Dependence of the induction time on supersaturation suggests that the mechanism of nucleation is primary. The correlation coefficient was obtained as 0.986. After formation, the nanoparticles were cross-linked with sodium persulfate as initiator and divinylbenzene as cross-linking agent. The SEM photos showed the formation of nanoparticles as well as their cross-linking. Such a finely porous layer can act as an effective support for active non-porous layers in applications such as gas separation. Also, based on the practical results, it was determined that for pressure equal 7 bar, temperature of 70 °C, membrane thickness of 1.15 mm and polybutadiene to divinyl benzene ratio of 1.5, the relative separation will be 93.58.

Keywords: Polybutadiene Nanoparticles, Nucleation, Induction Time, Cross-linking

INTRODUCTION

1. Nanoparticles

Induction crystallization is carried out when a secondary solvent, known as an anti-solvent, is added to the solution to reduce the solubility of a solute, resulting in a phase change. A burette is filled with the anti-solvent and its addition takes place dropwise, allowing 5 minutes for mixing, homogenizing and possible nucleation. To the best of our knowledge, Ghader et al. synthesized and studied the nucleation mechanism of silver nanoparticles for the first time using the reactive crystallization method [1-2]. We also synthesized these nanoparticles using the same method and compared the induction time with and without using anti-solvent [3]. The results showed that the induction time decreased by increasing the anti-solvent percentage and supersaturation.

2. Literature Review

2-1. The Nucleation Mechanism

The classical nucleation theory predicts that there is a linear relation between lnt and $\frac{1}{(\ln S)^2}$ according to Eq. (1) [4]:

$$\ln t = \ln K + \frac{16\pi\gamma^3 V^2}{3(KT)^3(\ln S)^2} \quad (1)$$

We required diagrams similar to (Fig. 2) and (Fig. 3) to determine the nucleation mechanism. Then the results of the experiments were compared with the classical nucleation theory. According to this theory, a linear relationship between lnt and $\frac{1}{(\ln S)^2}$ is expected (Fig. 2). Good fit of a line with a positive slope shows that the primary nucleation mechanism applies.

We required a diagram similar to Fig. 3 to investigate the secondary nucleation. Assuming the nucleation rate as $B=KS^n$ and considering $t\propto\frac{1}{B}$, we have Eq. (2) as follows [4]:

$$\ln t = \ln K - n \ln S \quad (2)$$

Therefore, the degree of nucleation is obtained from the slope of the straight line, plotted between lnt v.s. lnS. Good fit of a line with a negative slope indicates that a secondary nucleation applies.

2-2. Polymers

Wang et al. prepared PEI/PCL@ PdNPs composite fiber catalyst with high activity to reduce 4-nitrophenol and 2-nitroaniline in the solution and it was reusable [5]. Zhu et al. prepared T-G hydrogels that showed good adsorption for organic dyes, and AuNP/T-G composite showed high catalytic activity for 4-NP [6]. Huang et al. studied poly vinyl alcohol/poly acrylic acid/Fe_3O_4/MXene@Ag nanoparticles composite nanofibers; the results showed the best catalytic performance to 4-nitrophenol and 2-nitroaniline [7]. Hou et al. designed a self-assembled hydrogel from cyclodextrin polymer/adamantine-modified poly acrylic acid. Results showed that the hydrogels possessed different mechanisms in the adsorption of the poisonous organic dye molecules [8].

3. Cross-linking of the Polymers

In the cross-linking process, the polymer chains are bonded together and each of them is called "lattice". In fact, a 3D polymeric lattice is formed when the polymer molecules are bonded together. As a result, the polymer chains lose part of their freedom of movement. Therefore, this polymer lattice will have a very high resistance to heat and will not easily melt down. Butadiene with the structure shown in (Fig. 1) can be polymerized and cross-linked with other

†To whom correspondence should be addressed.
E-mail: Manteghi@modares.ac.ir

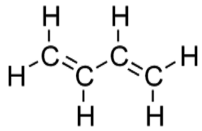

Fig. 1. Butadiene structure.

polymers due to the presence of two double bonds in it.

EXPERIMENTAL

1. Materials

Polybutadiene (M.W. between 1,530 and 2,070) was purchased from the Aldrich Co. (Germany). Toluene, ethanol, divinylbenzene were obtained from Merck (Germany). Sodium persulfate was provided from Central Drug House (India).

2. Formation of Polybutadiene Nanoparticles

Polybutadiene nanoparticles were produced in the first part of the research. Purchased polybutadiene was dissolved in toluene, and then ethanol was added to it as an anti-solvent dropwise until the solution became turbid.

3. Cross-linking the Nanoparticles

In the second part of the research, the produced nanoparticles were cross-linked as a step to fabricate the membranes. Sodium persulfate as an initiator and divinylbenzene as a cross-linking agent were added to the solution, and a white precipitation was formed by increasing the temperature to 60 °C. SEM photos show the relatively uniform surface, which has been created by cross-linking of nanoparticles (Figs. 5(a) and (b)).

RESULTS

1. Nucleation Mechanism

According to Fig. 2, a plot of lnt v.s. $\frac{1}{(\ln S)^2}$ (primary homogeneous nucleation model) has a positive slope and a correlation coefficient, R^2, of 0.986, while a plot of lnt v.s. lnS (a secondary nucleation model) has an R^2=0.925 (Fig. 3). The comparison clearly favors

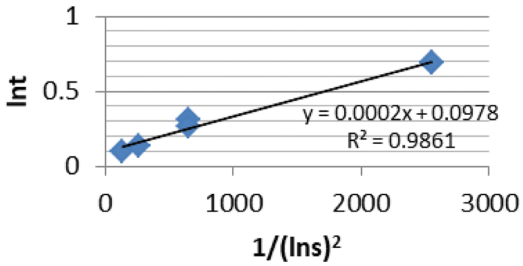

Fig. 2. Investigation of the primary nucleation mechanism.

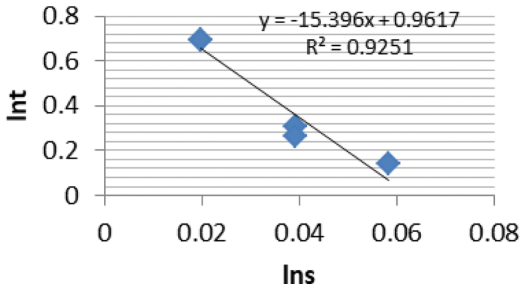

Fig. 3. Investigation of the secondary nucleation mechanism.

a primary homogeneous nucleation mechanism.

This is not unexpected, as when an anti-solvent is used, sudden increase of supersaturation should lead to exit from the metastable zone into the labile region, where bulk primary nucleation dominates.

2. Scanning Electron Microscopy (SEM)

2-1. Nanoparticles

SEM photos were taken to determine the size and shape of the particles. The photos confirm the formation of nanoparticles (Figs. 4(a), (b) and (c)).

2-2. Cross-linked Nanoparticles

Cross linking of polybutadiene nanoparticles was achieved by adding sodium persulfate as initiator and divinylbenzene as cross linking agent to the sol obtained as described above. The mixture was heated to 60 °C till a white precipitation of the cross-linked particles settled down. Fig. 5 shows the cross-linked polymer for-

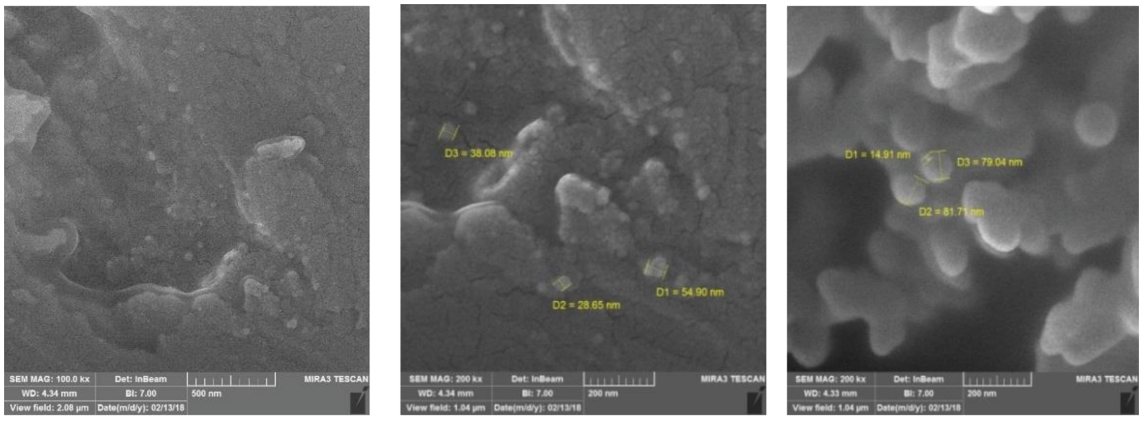

(a) (b) (c)

Fig. 4. SEM photos of polybutadiene nanoparticles.

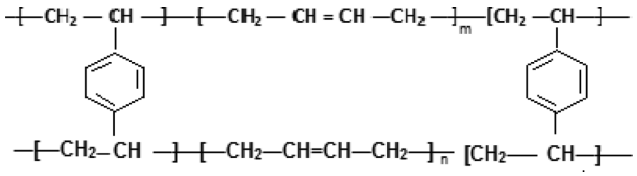

Fig. 5. Polybutadiene cross-linked by divinylbenzene.

mula (Figs. 6(a) and (b)) show electromicrographs of nanoparticles after cross-linking. As illustrated, a relatively uniform surface is created by adhering the nanoparticles together. This is a suitable candidate for supporting active layers for reverse osmosis or gas separation.

2-3. Attachment to the Thin Polyamide Layer

Thin polyamide layer was synthesized by first dissolving the polymer in ethanol, then evaporating the solvent at room temperature in a beaker. To attach the cross linked polybutadiene, the second was placed on the first after wetting the polyamide layer by a few drops of sodium persulfate and divinylbenzene.

The FT-IR and ATR analyses were performed to examine the functional groups and possible changes after structural modification. The IR spectrum of pure polybutadiene is shown in (Fig. 7(a)). The C=C bond produces a peak in the region of 1,653 cm^{-1}. The asymmetric and symmetric stretching vibrations of C-H are located at 2,942 and 2,861 cm^{-1}, respectively. Also, the peaks observed in the 1,454 cm^{-1}, 1,311 cm^{-1}, and 1,240 cm^{-1} are related to the C-H (scissoring), C-H (Rocking) and C-H (Wagging) vibrations, respectively. The vibration out of the plane belonging to the C-H bond is located at 728 cm^{-1}. The stretching vibrations of the O-H groups (related to the absorbed water) are shown in 3,218 cm^{-1}, and the bending vibration of C-H is placed in 966 cm^{-1} [9-11]. Fig. 7(b) shows the ATR spectrum of the polyamide membrane. In the ATR spectrum, the peak at 1,444 cm^{-1} is attributed to the N-H bending band and the low intensity peak observed in the 1,700-1,730 cm^{-1} region is related to the stretching vibration C=O, indicating the presence of amide groups in the structure. The peak at 3,006 cm^{-1} is the result of the N-H stretching vibration. The O-H stretching

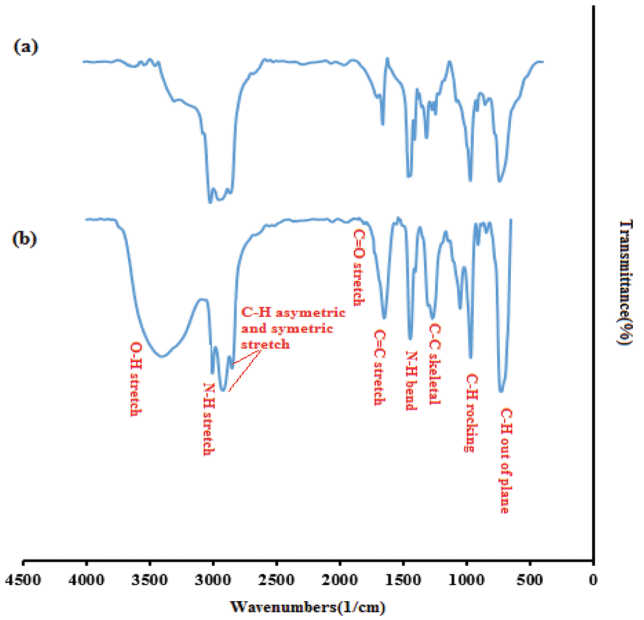

Fig. 7. (a) FT-IR spectrum of polybutadiene, (b) ATR spectrum of polyamide with cross-linked polybutadiene.

vibration gives a broad peak in 3,403 cm^{-1}. The band at 1,656 cm^{-1} corresponds to aromatic C=C stretching vibration and can indicate the presence of unsaturated aromatic carbon. The peak at 1,112 cm^{-1} represents the skeletal vibration of the C-C group. Moreover, the characteristic peaks at 968 cm^{-1} and 908 cm^{-1} regions are related to the stretching vibration of C-C=O group and the rocking vibration of the C-H bond, respectively. The out of plane C-H vibration appears at 728 cm^{-1}. Since the vibrational groups such as C=C and C-H are common in polyamide and poly-butadiene, overlapping between the locations appearing in the final membrane can be seen [12,13].

Fig. 8 illustrates the effects of operating pressure and membrane thickness on the relative separation of two carbon dioxide and helium gases in a membrane separation process. In this figure, the x-axis

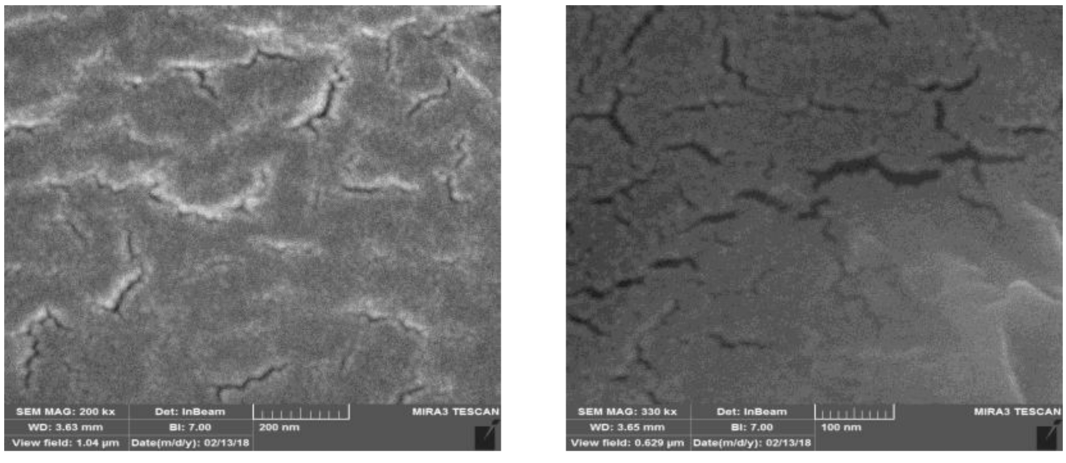

(a) (b)

Fig. 6. The SEM photos of polybutadiene cross-linked nanoparticles.

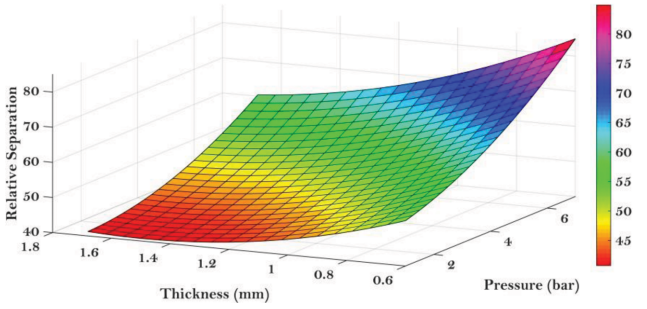

Fig. 8. Effects of pressure & thickness on the relative separation of carbon dioxide and helium gases.

represents the pressure changes in the range of one to seven bar, and the y-axis indicating the thickness of the membrane synthesized in the range of 0.6 to 1.7 millimeters. To create a more intuitive concept, the relative separation rate of the gas mixture based on the measurement of carbon dioxide concentration, after passing through the membrane, is shown as relative separation on the z axis. In this figure, for all pressure values, the decrease in membrane thickness has always led to a significant increase in the relative separation rate. This separation was carried out at low pressures up to forty-nine percent, with increasing pressure at lower membrane thicknesses of up to eighty-three percent (83%).

CONCLUSION

The experiments and SEM photos show that polybutadiene nanoparticles can be produced using ethanol as an anti-solvent. The investigation of the nucleation mechanism diagrams supports the primary nucleation mechanism. The produced nanoparticles were cross-linked in order to fabricate the membrane support layer. The SEM photos show the formation of a relatively uniform surface ready for attachment to a non-porous polyamide layer to synthesize membranes with suitable selectivity, mechanical resistance and permeability. The attached layers were characterized by FT-IR and ATR. It was determined that for pressure equal to 7 bar, temperature of 70 °C, membrane thickness of 1.15 mm and polybutadiene to divinyl benzene ratio of 1.5, the relative separation will be 93.58.

REFERENCES

1. S. Ghader, M. Manteghian, M. Kokabi and R. S. Mamoory, *Chem. Eng. Technol.*, **30**, 1129 (2007).
2. S. Ghader, M. Manteghian, M. Kokabi and R. S. Mamoory, *Pol. J. Chem.*, **81**, 1555 (2007).
3. F. Sayyahpour, M. Manteghian and S. Ghader, *IChEC*, 24 (2014).
4. J. W. Mullin, *Crystallization*, 4th Ed., Butterworth-Heinemann, London (2001).
5. C. Wang, J. Yin, S. Han, T. Jiao, Z. Bai, J. Zhou, L. Zhang and Q. Peng, *Catalysts*, **9**, 559 (2019).
6. J. Zhu, R. Wang, R. Geng, X. Zhang, F. Wang, T. Jiao, J. Yang, Z. Bai and Q. Peng, *RSC Adv.*, **9**, 22551 (2019).
7. X. Huang, R. Wang, T. Jiao, G. Zou, F. Zhan, J. Yin, L. Zhang, J. Zhou and Q. Peng, *ACS Omega*, **4**, 1897 (2019).
8. N. Hou, R. Wang, R. Geng, F. Wang, T. Jiao, L. Zhang, J. Zhou, Z. Bai and Q. Peng, *Soft Matter*, **15**, 6097 (2019).
9. M. M. A. Nikje and H. Hajifatheali, *J. Elastomers Plast.*, **45**, 457 (2013).
10. F. Wang, L. Chang, Y. Hu, G. Wu and H. Liu, *Polymers*, **11**, 791 (2019).
11. R. Wang, F. Tsow, X. Zhang, J. H. Peng, E. Forzani and Y. Chen, *Sensors*, **9**, 5655 (2009).
12. C. J. Gabelich, J. C. Frankin, F. W. Gerringer, K. P. Ishida and I. M. Suffet, *J. Membr. Sci.*, **258**, 64 (2005).
13. K. M. D. Medeiros, E. M. Araújo, H. d. L. Lira, D. d. F. Lima and C. A. P. d. Lima, *Mat. Res.*, **20**, 308 (2017).